Asian Journal of Chemistry; Vol. 36, No. 11 (2024), 2583-2592

ASIAN JOURNAL OF CHEMISTRY

https://doi.org/10.14233/ajchem.2024.32582

Charge Transfer Interaction Dynamics between 2-Methyl-8-hydroxyquinoline and 2,4-Dinitrophenol: Synthesis, Spectroscopic Characterization, DNA Binding and DFT Studies

V. SUNDARPAL[1], J. SRINU[1], G. SAILAJA[1], B. SHASHI KANTH[2], V. KIRAN KUMAR[3], B. MANOHAR[1], P. SOMESHWAR[1], N. RAJITHA[4] and B. YADAGIRI[1,*]

[1]Department of Chemistry, Osmania University, Hyderabad-500007, India
[2]Department of Chemical Technology, Loyola Academy, Hyderabad-500010, India
[3]Department of Chemistry, IIT Hyderabad, Kandi, Sangareddy-502285, India
[4]Department of Chemistry, Nizam College, Hyderabad-500001, India

*Corresponding author: E-mail: bygiriou@gmail.com

Received: 27 August 2024; *Accepted*: 14 October 2024; *Published online*: 30 October 2024; AJC-21793

A novel charge transfer (CT) complex was formed by combining the electron-acceptor 2,4-dinitrophenol (DNP) with the electron-donor 2-methyl-8-hydroxyquinoline (MHQ). The complex obtained was further characterized using both experimental and theoretical methods. The Benesi-Hildebrand equation can be utilized to determine various spectroscopic physical measurements such as the molar absorptivity (ε_{CT}) and formation constant (K_{CT}). The CT complex has a stoichiometry of 1:1. Multiple spectroscopic methods were employed to investigate the resultant solid compound. The existence of charge and proton transfer in the resultant complex was confirmed by FT-IR, ^{1}H NMR, SEM-EDX and powder-XRD studies. An electron absorption spectroscopy examination was done to analyze the complex DNA binding capability. The resulting complex was determined to have an intercalative binding mechanism, with an intrinsic binding constant (K_b) value of $4.2 \times 10^6\ M^{-1}$. The experimental results were corroborated by performing theoretical calculations using DFT using a CAM-B3LYP/6-31G(d,p) basis set. The geometrical parameters, electrostatic potential maps (MEPs) and Mullikan charges were computed and examined in agreement with the experimental observations. In addition to electron transmission, the stability of the complex is influenced by the presence of a hydrogen bond.

Keywords: Charge transfer complex, Proton transfer, DFT calculation, DNA binding.

INTRODUCTION

Mulliken [1] and Emslie *et al.* [2] established a methodology termed charge transfer (CT), which comprises an acceptor and donor to establish a CT complex. When a partial migration occurs during the electronic charge transfer from donor molecule D to acceptor molecule A, this process is referred to as the CT-type [3,4]. The CT complexes can be distinguished by analyzing their absorption spectrum, which reveals a unique absorption band that is not present in the spectra of their individual acceptor and donor atoms [5]. In the process, there is a transfer of charge from the highest occupied molecular orbital (HOMO) of the donor to the lowest unoccupied molecular orbital (LUMO) of the acceptor. This leads to the formation of a new absorption band [6,7]. The CT complexes have a crucial part in biological systems, since they contribute to antifungal, antibacterial, antimalarial effects and DNA-binding [8-11].

Quantum chemistry utilizes DFT to gain valuable insights into molecular structures and their spectral characteristics [12]. The polarizable continuum model (PCM) can be used to determine the geometric properties of CT complexes [13,14]. The integration of theories [15] with spectrum analysis methods has been employed to characterize CT and hydrogen-bonded compounds. Nitrogen containing heterocyclic compounds provide as electron donors in the formation of charge transfer complexes. Quinoline derivatives have attracted considerable attention as biomolecules due to their pharmacological characteristics [16,17]. Compounds belonging to the quinoline family have medicinal characteristics that assist with asthma, bacterial

infections, fungal infections, malaria, viral infections and inflammation.

2-Methyl-8-hydroxyquinoline (MHQ), a quinoline derivative with methyl substitution, has been used in several material and biological applications [18]. Phenol is a chemical that has been extensively explored due to its ability to form complexes with oxygen and nitrogen bases through hydrogen bonding. These complexes possess the capacity to constantly alter the interactions between donors and acceptors. The use of 2,4-dinitrophenol (DNP) can be beneficial for study in the fields of chemistry and biology. In addition, it can be used as a reagent for developing metal complexes that exhibit powerful hydrogen bonding interactions [19]. When working with CT complexes, one can utilize it as an electron acceptor.

In light of their biological and pharmacological importance of proton and charge transfer interactions, this study provides electronic absorption data on the proton transfer process in methanol between MHQ (proton receiver) and DNP (proton donor). The elemental composition of the CT complex was analyzed using FT-IR, UV-visible, powder X-ray diffraction, ^{1}H NMR and SEM-EDX spectroscopies. This study includes the impact of solvent (MeOH) by using the polarizable continuum model (PCM) along with DFT study.

EXPERIMENTAL

2,4-Dinitrophenol (DNP) and 2-methyl-8-hydroxyquinoline (MHQ) (Merck) were utilized without any further purification. A high-quality grade methanol from Merck, specifically designed for analysis purposes, was used to prepare the primary solution. Calf thymus DNA (*ct*-DNA) from Sisco Research Laboratory, Tris buffer from Mole chem and sodium chloride with a purity of 99.50% were used.

Preparation of standard solution: A standard stock solution was prepared by completely dissolving a weighed DNP and different quantities of MHQ in methanol. The MHQ and DNP were dissolved in MeOH to obtain 10^{-2} M solution. The initial stock solutions were diluted further to attain a final concen-tration of 10^{-4} M. The original solution was diluted with the same solvent to obtain different concentration solutions of 1×10^{-4} M, 1.5×10^{-4} M, 2×10^{-4} M and 2.5×10^{-4} M.

Preparation of solid CT complex: The solutions of MHQ (0.139 g) and DNP (0.186 g) were carefully prepared in MeOH and then mixed carefully in order to obtain a yellow solution. After being stirred continuously for 1 h, the solution was left to gradually evaporate at room temperature. The solid was washed with a small quantity of MeOH to remove any residual unreacted compounds and subsequently dried under vacuum using anhydrous $CaCl_2$.

***ct*-DNA stock solution:** The stock solution of DNA was prepared by dissolving 50 mM NaCl and 5 mM Tris-HCl in double distilled water at 25 ºC. The purity of the DNA solution was evaluated by quantifying the UV-vible absorbance at 260 and 280 nm, which should fall within the range of 1.8 to 1.9. The Ct-DNA sample was devoid of any protein contaminants [20]. Using absorption spectroscopy, the proportion of Ct-DNA was determined by measuring the absorbance at 260 nm, with a molar absorptivity of 6600 M^{-1} cm^{-1}. The solution was held at 3-4 ºC and stored for 3-4 days. Throughout the entire experiment, the chemical was dissolved in a buffer solution made up of equal parts Tris-HCl and methanol. The titration tests employed DNA concentrations ranging from 0 to 10 µM, while keeping the complex concentration constant.

Characterization: An SEM was used to analyze the surface of [(MHQ):(DNP)] complex, utilizing a Zeiss Evo18 scanning electron microscope. The chemical composition of CT complex was measured precisely using a SEM-EDX spectrometer. The ^{1}H NMR analysis was performed with a BRUKER 400 MHz NMR spectrometer employing DMSO-d_6 as solvent. The FT-IR spectra were obtained using BRUKER Alpha Spectrometers employing KBr discs method. The UV-absorption spectra of DNP, MHQ and the [(MHQ):(DNP)] complex were measured in the 200-800 nm range using a SHIMADZU UV-2600 spectrophotometer.

Computational calculations: The computational parameters as well as the energy of LUMO and HOMO were carried out *via* Gaussian 09W [21]. Optimizing the chemical structure of the CT complex involved the CAM-B3LYP function and the 6-31G(d,p) basis set to enhance the optimization process. The software program Gauss view [22] was used to visually portray the estimated structures, including the depiction of the HOMO, LUMO and the molecular electrostatic potential (MEP).

RESULTS AND DISCUSSION

Morphological studies: The surface morphology and elemental content of the [(MHQ):(DNP)] (CT complex) were examined by SEM-EDX analysis. The scanning electron micrographs (Fig. 1) at different magnification illustrate that the product exhibits microstructures resembling translucent sheets. By examining the EDX spectra (Fig. 1d), it was shown that the CT complex consisted of carbon, nitrogen, oxygen, and bromine elements only.

The powder X-ray diffraction pattern obtained for the semi-crystalline CT combination of MHQ with DNP is shown in Fig. 2. The findings indicate that the newly formed [(MHQ):(DNP)] CT complex possesses semi-crystalline properties, as distinct and well-defined Bragg peaks are present at certain 2θ angles. The Debye-Scherrer's formula [18] was used to determine the particle size distribution of the complex by analyzing the line with the highest intensity compared to the other lines.

$$D = \frac{0.94\lambda}{\beta\cos\theta} \quad (8)$$

where λ is the X-ray wavelength (λ = 0.15406 nm); D is the size of the crystal in nm; β is the full width at half maximum of the crystal; θ is the position of diffraction peak and 0.94 represents the Scherrer constant. The particle sizes of DNP, MHQ and the [(MHQ):(DNP)] complex are 14.68 nm, 15.61 nm and 22.14 nm, respectively, as estimated.

^{1}H NMR spectral studies: The ^{1}H NMR spectra of MHQ and [(MHQ):(DNP)] were acquired in DMSO-d_6 solvent. Table-1 of the intricate spectrum reveals that the DMSO proton is detected at a chemical shift of δ 2.5 ppm. The emergence of ancillary signals in the spectrum indicates that the complex is

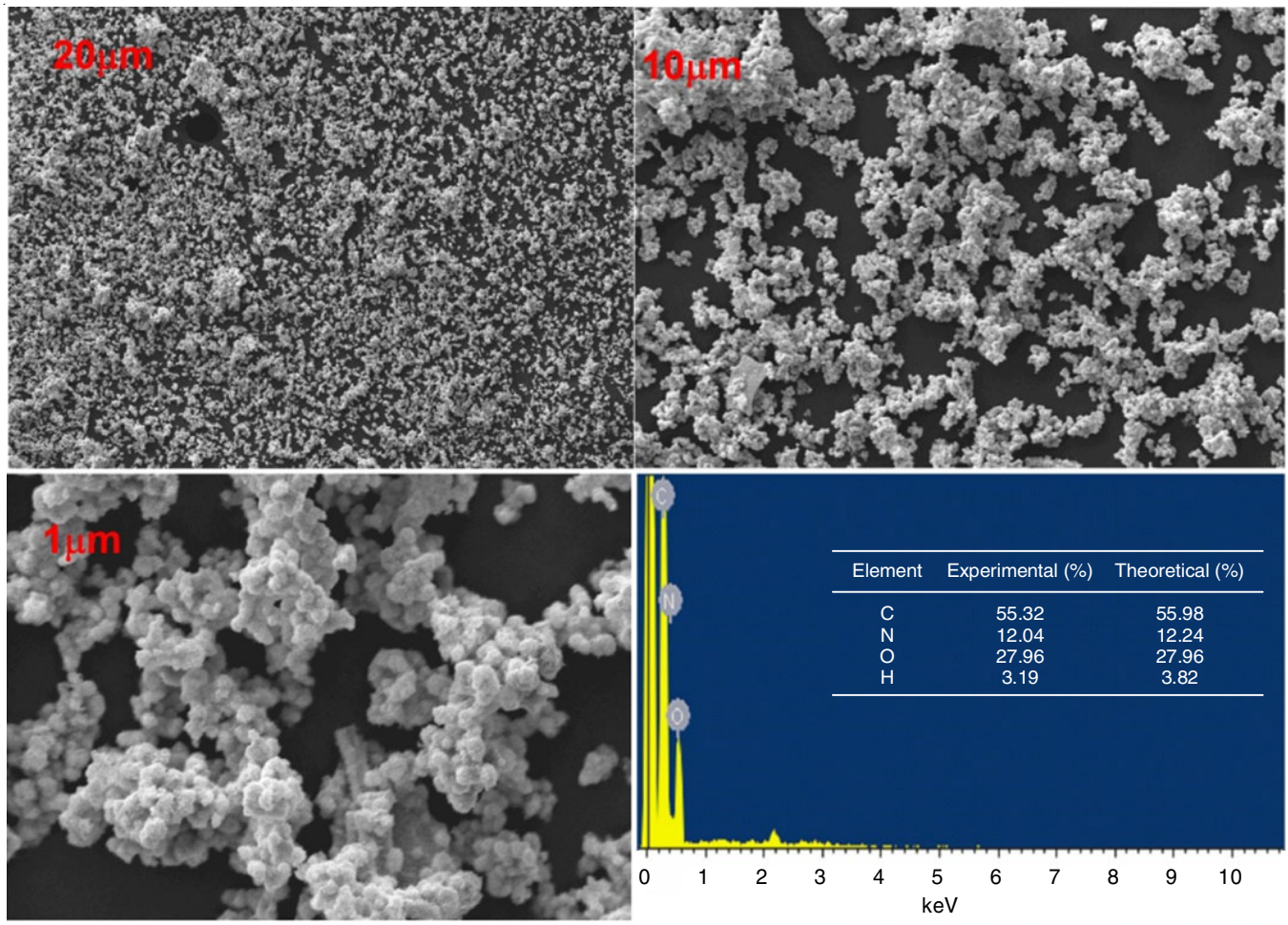

Fig. 1. SEM images and EDX spectrum [(MHQ)(DNP)] complex

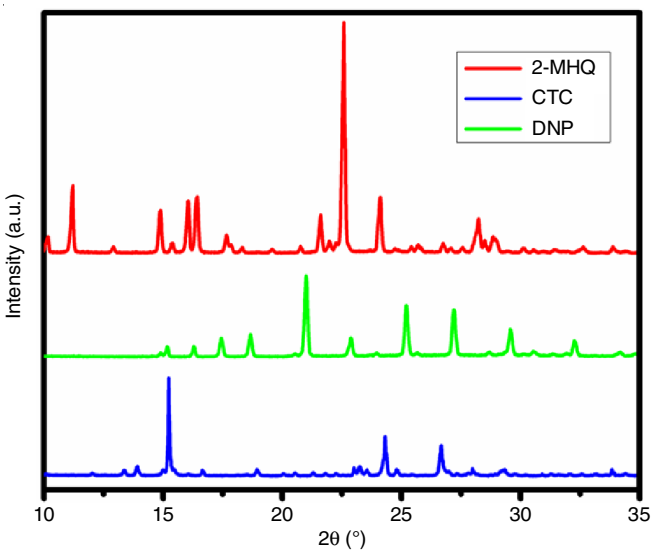

Fig. 2. Powder XRD spectra of MHQ, DNP and [(MHQ)(DNP)] complex

developing. The quinoline molecule contains a methyl group that consists of three protons. One of these protons is specifically designated as number one and has a chemical shift value of δ 2.72 ppm. The peaks observed at δ 6.00 and 8.00 ppm are attributed to the presence of aromatic protons in the molecule.

TABLE-1
^{1}H NMR SPECTRAL DATA OF MHQ AND CT COMPLEX

Compound	Chemical shift, δ (ppm)	Assignments
MHQ	7-8.5	(d, t, 5H, Ar-H)
	9.39	(s, 1H, OH of MHQ)
	2.69	(s, CH_3 of MHQ)
	8.20, 7.41, 7.34, 7.07	(d, t, 5H of MHQ Ar-H)
[(MHQ)(DNP)]	2.72	(s, CH_3 of MHQ)
	8.18, 7.43, 7.36	(s, 3H of DNP Ar-H)
	3.35	(s, 1H of NH proton transfer)

d-doublet; s-singlet

The formation of the NH^+ center happens when the phenolic proton of DNP is transferred to the nitrogen atom of pyridine ring in MHQ, is thought to be responsible for the identification of a broad resonance signal at δ 3.35 ppm.

FTIR spectral studies: Fig. 3 illustrates the FT-IR spectra of DNP, MHQ and [(MHQ):(DNP)] complex. Table-2 shows a brief overview of the primary band designations. The impact of MHQ and DNP resulted in the significant changes in the frequency and intensity of the CT complex spectrum. Complexation causes the addition of charge and makes it easier for protons to be exchanged. The formation of the [(MHQ):(DNP)] complex is strongly supported by the fact that the complex show

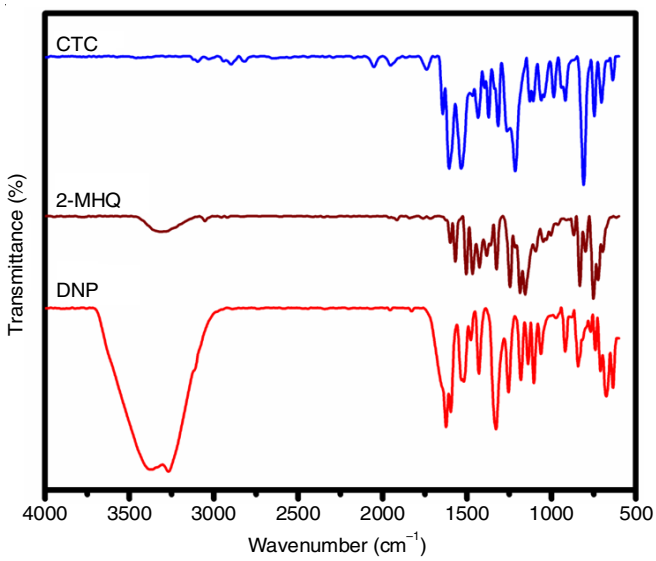

Fig. 3. Experimental FT-IR spectra MHQ, DNP and [(MHQ)(DNP)] complex

TABLE-2
THE EXPERIMENTAL INFRARED FREQUENCIES (cm^{-1}) OF MHQ, DNP AND CTC

Assignments	MHQ	DNP	CTC
$\nu(CH)_{aromatic}$	2945		3031
$\nu(CH)_{aliphatic}$	2965		3096
ν(O-H---N)			2907
ν(OH)		3364	
$\nu(C=C)_{aromatic}$	1596	1556	1606
ν(C=N)	1515		1535
ν(C-C)	1104	1089	1129
$\nu(NO_2)$		1328	1372
δ(C-N)	1371		1304
$\nu(NH^+)$			1644

the prominent IR bands of the donor and the acceptor simultaneously [10]. The absence of the OH group in the DNP complex indicates that proton transfer for hydrogen bonding occurred, resulting in the OH group migrating towards the basic centers of the donor MHQ. The complex spectrum also shows an increase in the stretching vibrational frequencies of ν(C=C), (C-N) and (C=N) at 1606, 1304 and 1535 cm^{-1}, respectively, compared to the peaks at 596, 1371 and 1515 cm^{-1} observed in the spectrum of free MHQ. On the other hand, a weak broad peak at 2907 cm^{-1} indicates the transfer of protons from the OH group of DNP to the nitrogen atom in the ring of MHQ, which is caused by the complex (NH^+).

Studies of solution state

Stoichiometric ratio of complex: Using Job's method, the stoichiometric ratio of the CT complex was determined in MeOH medium at 450 nm [23]. The highest absorbance was achieved at a mole ratio of 0.5, suggesting that the complex has a ratio of 1:1 [(MHQ):(DNP)] (Fig. 4a), whereas the photometric titration curve in methanol is illustrated in Fig. 4b [24].

Detection of CT band: Fig. 5 presents the UV-vis spectra of DNP, MHQ and CT complex, acquired in methanol within the wavelength range of 200-700 nm. When the acceptor and donor solutions exhibited minimal light absorption in specific areas, their combination led to a distinct colour change and the emergence of extra bands. The intricate spectra exhibited two charge transfer bands in MeOH at 450 and 345 nm. The charge transfer peak [25] was identified with the longest wavelength, measuring 450 nm. As a result, the CT complex among DNP and MHQ was formed, as illustrated in **Scheme-I**. Appearance of the new CT band indicating the movement of a lone pair from MHQ to DNP. The interaction between MHQ and DNP is enhanced through the formation of hydrogen bonds.

Molar absorptivity (ε_{CT}) and association constant (K_{CT}): The molar absorptivity (ε_{CT}) and association constant (K_{CT}) were calculated at room temperature using the Benesi-Hildebrand equation [26] (Table-3).

$$\frac{C_a C_d}{A} = \frac{1}{K_{CT}\varepsilon} + \frac{(C_a - C_d)}{\varepsilon} \quad (1)$$

where A is the absorbance at 450 nm in methanol, specifically for the MHQ to DNP ratio; C_d and C_a represent the initial concentrations of MHQ (at varied concentration) and DNP (at fixed

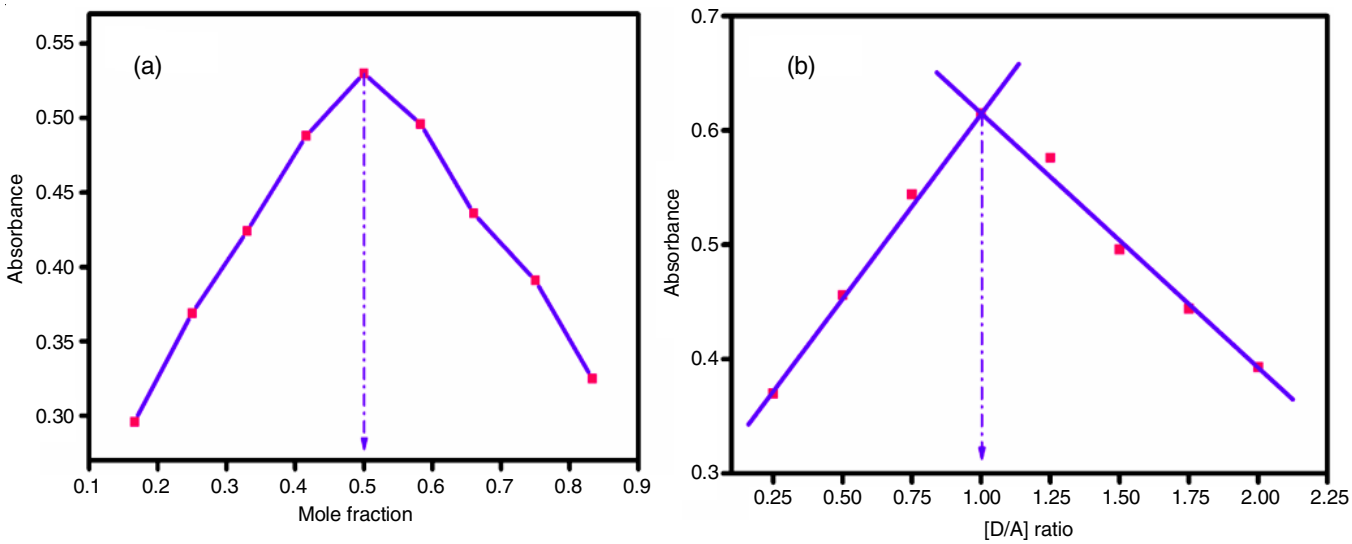

Fig. 4. (a) Job's plot (b) Spectrophotometric plot of CT complex in MeOH

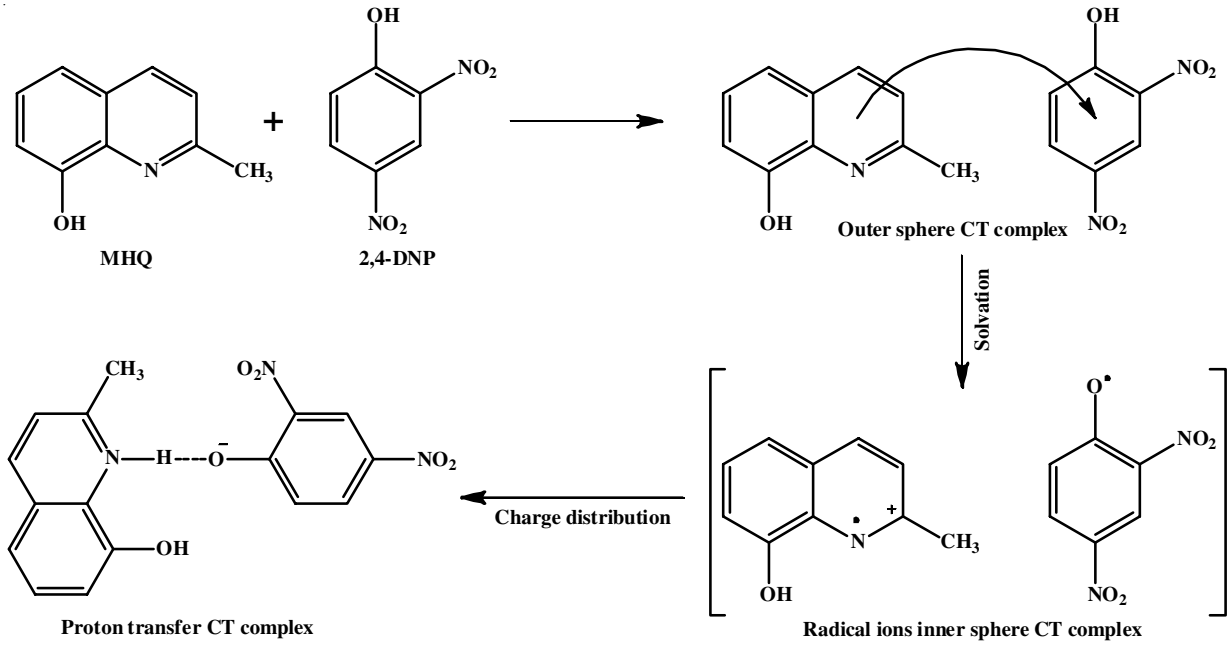

Scheme-I: Proposed proton and charge transfer mechanism between MHQ and DNP

TABLE-3
BENESI-HILDEBRAND DATA FOR 1:1 CT COMPLEX AT 25 °C

C_a	C_d	A	C_aC_d/A	$C_a + C_d$	$(C_aC_d/A) \times 10^6$	$(C_a + C_d) \times 10^3$
0.001	0.0050	0.791	6.32×10^6	0.0060	6.32	6.0
0.001	0.0045	0.763	5.89×10^6	0.0055	5.89	5.5
0.001	0.0040	0.716	5.58×10^6	0.0050	5.58	5.0
0.001	0.0035	0.699	5.00×10^6	0.0045	5.00	4.5
0.001	0.0030	0.665	4.51×10^6	0.0040	4.51	4.0
0.001	0.0025	0.648	3.85×10^6	0.0035	3.85	3.5
0.001	0.0020	0.618	3.23×10^6	0.0030	3.23	3.0
0.001	0.0010	0.489	2.04×10^6	0.0020	2.04	2.0

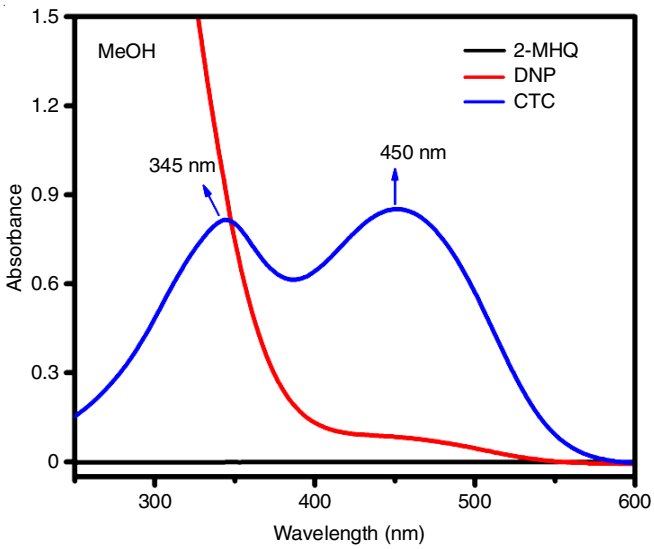

Fig. 5. UV-vis spectra of MHQ, DNP and [(MHQ)(DNP)] in MeOH medium

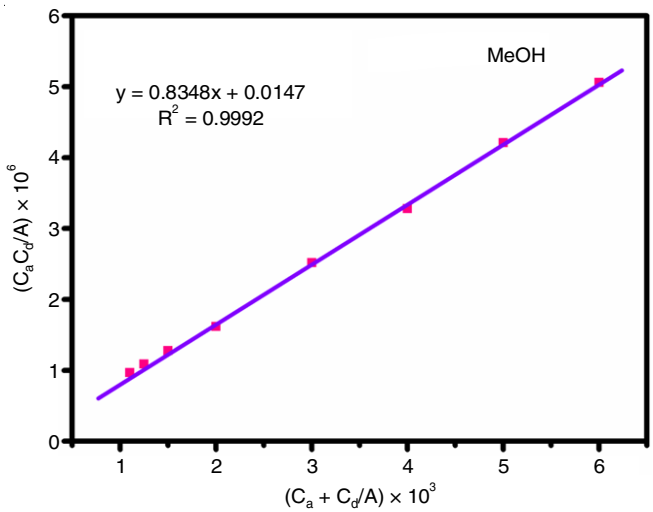

Fig. 6. Benesi-Hildebrand plots at room temperature

concentration), respectively. When the $C_a \times C_d 10^6$ values were plotted against the sum of C_a and C_d, a linear relationship was seen, suggesting the formation of a 1:1 complex (Fig. 6). Table-4 presents the formation constants, extinction coeffi-cients and wavelengths of CT molecule, indicating that the CT-complex exhibits remarkable stability, as evidenced by the elevated molar extinction coefficient and association constant.

Determination of physical parameters: The electronic spectral analysis was used to derive and investigate the spectroscopic physical features of [(MHQ):(DNP)]. The equations are provided as follows:

TABLE-4
FORMATION CONSTANTS, MOLECULAR EXTINCTION COEFFICIENTS AND OTHER PHYSICAL PARAMETERS OF CT COMPLEX

Solvent	λ_{max} (nm)	$K_{CT} \times 10^2$ (L mol^{-1})	$\varepsilon_{CT} \times 10^2$ (L mol^{-1} cm^{-1})	-ΔG° (kJ/mol)	E_{CT} (eV)	W (eV)	I_D (eV)	f	R_N
MeOH	450	5.25	99.60	-21.20	2.76	34.8	39.5	3.14	0.788

(i) Dissociation energy (W): Using eqn. 2 [27], the complex dissociation energy (W) was accurately calculated. To obtain this information, the acceptor and donor's E_{CT}, I_D and EA were calculated.

$$W = I_D - EA - E_{CT} \quad (2)$$

(ii) Ionization energy (IP): The ionization energy (IP) of the CT complex in MeOH solvent was determined using eqn. 3 as provided by Piganatro & Aloisi [28]:

$$IP = 5.76 + 1.53 \times 10^{-4} \nu_{CT} \quad (3)$$

(iii) Computation of E_{CT}: The donor-acceptor association energy (E_{CT}) was calculated by using Angew & Briegleb's equation [27]:

$$E_{CT} = \frac{1243.667}{\lambda_{CT}} \quad (4)$$

(iv) Resonance energy (R_N): The value of the complex resonance energy (R_N) in methanol was calculated using eqn. 5 [29]:

$$\varepsilon_{CT} = \frac{7.7 \times 10^4}{h\nu_{CT} / [R_N] - 3.5} \quad (5)$$

(v) Gibb's free energy (ΔG°): The complex standard Gibb's free energy change (ΔG°) was calculated by using eqn. 6 [27]:

$$\Delta G^\circ = -RT \ln K_{CT} \quad (6)$$

(vi) Oscillator strength (*f*): The oscillator strength (*f*) is a dimensionless variable that measures the probability of a charge transfer (CT) band transition and can be determined using eqn. 7 [30]:

$$f = 4.32 \times 10^{-9} [\varepsilon_{max}. \Delta\nu_{1/2}] \quad (7)$$

All the measurements for the physical parameters are provided in Table-4 also.

DNA binding studies: This study explored the binding affinity by analyzing the effect of increasing *ct*-DNA concentration on the absorbance of CT complex while keeping the concentration of CT complex constant. The absorption spectra of complex following its interaction with *ct*-DNA are shown in Fig. 7. By utilizing the blue shift and hypochromic spectra, one can ascertain the intercalation mechanism between [(MHQ):(DNP)] and *ct*-DNA. The absorbance decreased as the DNA concentration increased using [(MHQ):(DNP)] suggesting that there is further evidence of a robust DNA binding mechanism. The Wolfe-Shimmer equation was employed to calculate the intrinsic binding constant (K_b) based on the absorption data.

$$\frac{[DNA]}{(\varepsilon_a - \varepsilon_f)} = \frac{[DNA]}{(\varepsilon_b - \varepsilon_f)} + \frac{1}{K_b(\varepsilon_b - \varepsilon_f)} \quad (9)$$

where K_b = intrinsic binding constant; [DNA] = *ct*-DNA concentration; ε_a = apparent coefficient; ε_f and ε_b = extinction coefficients for unbound and bound DNA, respectively. The value of K_b can be calculated by dividing the slope by the intercept obtained from a graph of DNA/($\varepsilon_a - \varepsilon_f$) *vs.* [DNA]. The complex has an intrinsic binding constant (K_b) ratio of 4.2×10^6 M^{-1}. The investigation of DNA binding has demonstrated that [(MHQ):(DNP)] possesses planarity and a π-structure, suggesting the possibility of DNA intercalation.

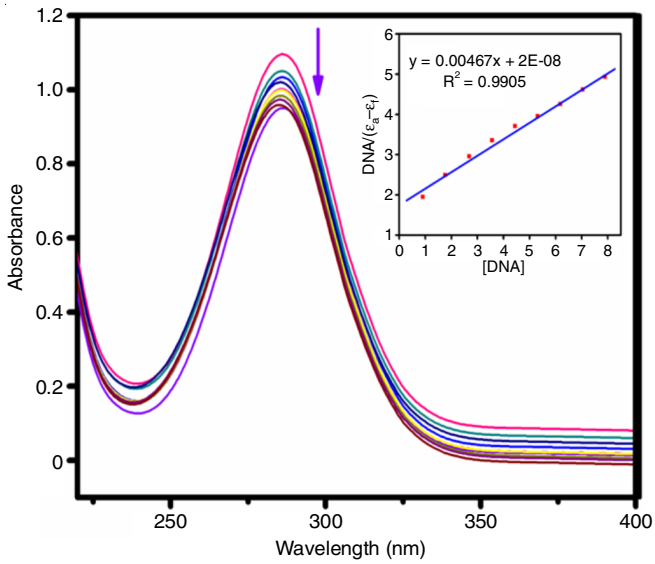

Fig. 7. Absorption spectra of [(MHQ)(DNP)] in Tris-HCl buffer upon addition of Ct-DNA. [Compound] =25 μM, [DNA] = 0-10 μM DNA concentration

Computational studies

Bond parameters: The optimized structures of DNP, MHQ and resulting [(MHQ):(DNP)] are displayed in Fig. 8. The structures are shown for both the gas phase and a solution in PCM (methanol). Complexation causes the changes in bond lengths in both the reactants and the complex as a result of proton and charge transfer. The distance between the atoms C4 and C5 in the complex increased to 1.441 Å and 1.450 Å in the gas and PCM, respectively, compared to 1.411 Å and 1.394 Å for free DNP (Table-5). In both states, the complex showed a decrease in the length of the C-O bond to 1.285 Å and 1.271 Å, respectively, compared to the free DNP, which had C5-O16 bond lengths of 1.346 Å and 1.316 Å. To the hydrogen bond, the separation between O16 and H17 increased to 1.517 Å in the gas phase and 1.796 Å in PCM, as opposed to 0.991 Å and 0.976 Å for DNP alone. This event occurs as a result of the rearrangement of protons in the hydrogen bonding of CT complex. The existence of the N38-H35 bond is observed in the CT-complex, with a measured length of 1.484 Å. Nevertheless, the free MHQ completely lacks this link. It offers significant assistance in transferring the DNP proton from O-H to the ring nitrogen of MHQ, both in the gas phase and in PCM.

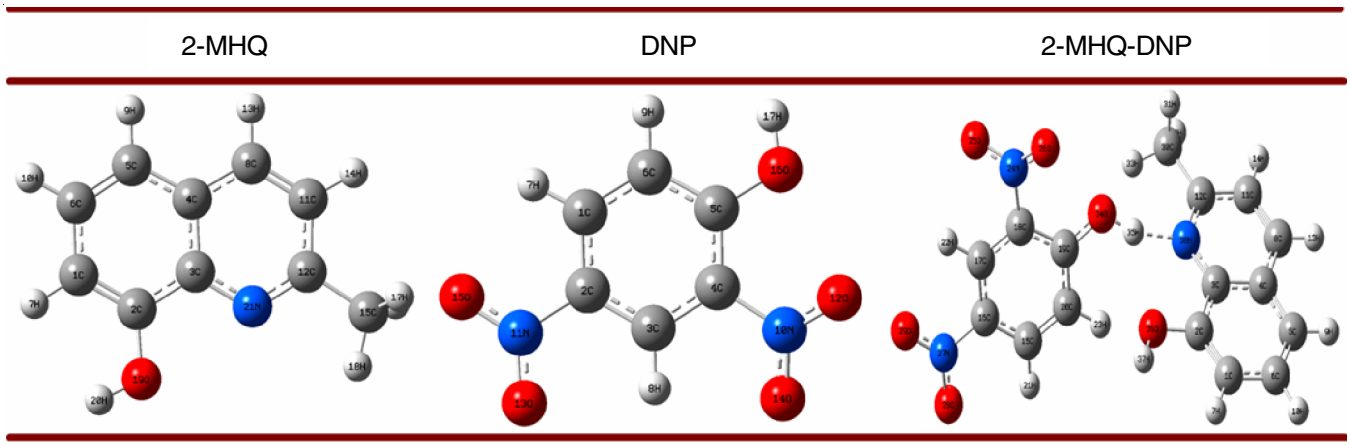

Fig. 8. Optimized geometries in gas phase MHQ, DNP and [(MHQ)(DNP)] complex

TABLE-5
OPTIMIZED BOND LENGTH VALUES OF
MHQ, DNP AND [(MHQ)(DNP)] COMPLEX

Bond length (Å)	MHQ	DNP	CTC	
			Gas	PCM
C1-C2	1.375	–	1.382	1.381
C2-C3	1.387	–	1.379	1.376
C3-C4	1.386	–	1.401	1.402
C4-C5	1.416	–	1.421	1.424
C5-C6	1.415	–	1.419	1.420
C3-N21	1.331	–	1.324	1.327
C12-N21	1.344	–	1.339	1.340
C11-C12	1.416	–	1.421	1.425
C11-C8	1.415	–	1.419	1.426
N38-H35	–	–	1.484	1.489
C1-C2	–	1.400	1.403	1.406
C2-C3	–	1.377	1.389	1.392
C3-C4	–	1.392	1.394	1.396
C4-C5	–	1.411	1.422	1.427
C5-C6	–	1.404	1.416	1.421
C2-N11	–	1.455	1.456	1.458
N11-O15	–	1.252	1.264	1.262
N11-O13	–	1.253	1.266	1.268
C4-N10	–	1.442	1.460	1.464
N10-O12	–	1.244	1.265	1.268
C5-O16	–	1.346	1.336	1.331
O16-H17	–	0.991	1.437	1.451

TABLE-6
OPTIMIZED BOND ANGLE VALUES OF
MHQ, DNP AND [(MHQ)(DNP)] COMPLEX

Bond angles (°)	MHQ	DNP	CTC	
			Gas	PCM
C1-C2-C3	122.6	–	123.9	123.2
C3-C4-C5	119.7	–	120.6	120.1
C11-C8-C4	118.3	–	119.6	120.1
C3-C4-N21	123.4	–	124.7	125.2
C11-C12-N21	121.4	–	119.7	119.2
C15-C12-N21	121.8	–	122.2	122.9
C2-C3-N21	120.9	–	121.1	121.8
C1-C2-O19	124.1	–	124.3	124.7
C3-N21-H35	–	–	119.9	120.1
C2-C1-C6	–	119.3	119.2	119.1
C1-C6-C5	–	120.7	120.9	121.3
C4-C5-C6	–	118.2	117.6	117.4
C2-C3-C4	–	118.4	119.1	119.9
O15-N11-O13	–	124.2	123.9	123.1
C2-N11-O13	–	118.1	118.2	118.9
C2-N11-O15	–	117.7	117.7	117.9
O14-N10-O12	–	122.5	123.1	123.9
C4-N10-O14	–	118.1	119.6	120.2
C4-N10-O12	–	118.1	117.2	116.8
C4-C5-O16	–	124.5	120.5	120.2
C6-C5-O16	–	117.1	121.8	122.2
C5-O16-H17	–	110.6	123.5	124.1

The optimal binding angles between the gas and the PCM are indicated in Table-6. Studies have shown that the bond angles that are in close proximity to the hydrogen bonding bridge are the most significant. During the complexation in both states, the bond angles C11-N21-C12 decrease to 119.7º and 119.2º, respectively, which is in comparison to the angle of 121.4º for MHQ alone. This observation suggests that hydrogen bonding and proton transfer contribute to the accumulation of reduced charge in the donor site, in addition to charge transfer association. The complex alters the bond angles of C5-O16-H17 for the acceptor moiety, increasing them from 110.6º in free DNP to 133.8º in the gas phase and 130.2º in PCM. The changes in bond angles give solid evidence that the new complex contains both protons and transferred charges.

Electrostatic potential maps (MEP): Fig. 9 displays the molecular electrostatic potential (MEP) maps of DNP, MHQ and the ratio of MHQ to DNP. If MHQ displays a red colour on the ring nitrogen, it can be categorized as a hydrogen acceptor and nucleophile. When examining DNP, the OH group exhibits a blue colour, indicating its role as an H-bond donor (electrophile). After analyzing the MEP of CT complex, it is clear that the red colour has vanished and substituted by blue colour in the quinoline ring. However, the red colour hinders the visibility of the DNP part by causing the blue colour to disappear. This indicates that DNP exhibits a significant ability to take substances, with the LUMO on O35 serving as the major site for acceptance. The MEP map demonstrated the existence of both charge accumulation and proton transport within the examined complex.

FMOs of the charge transfer complex: Fig. 10 shows the HOMO-LUMO maps of the [(MHQ):(DNP)] complex. In Fig. 11, the band gap energy (eV) between the gas and PCM

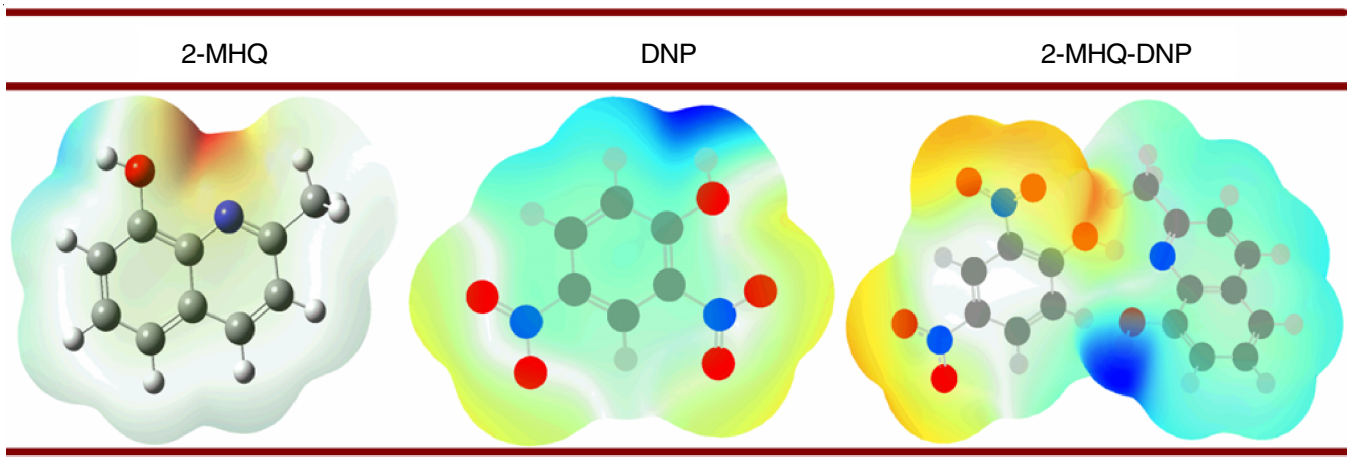

Fig. 9. Molecular electrostatic potential (MEP) maps of MHQ, DNP and [(MHQ)(DNP)] complex in gas phase

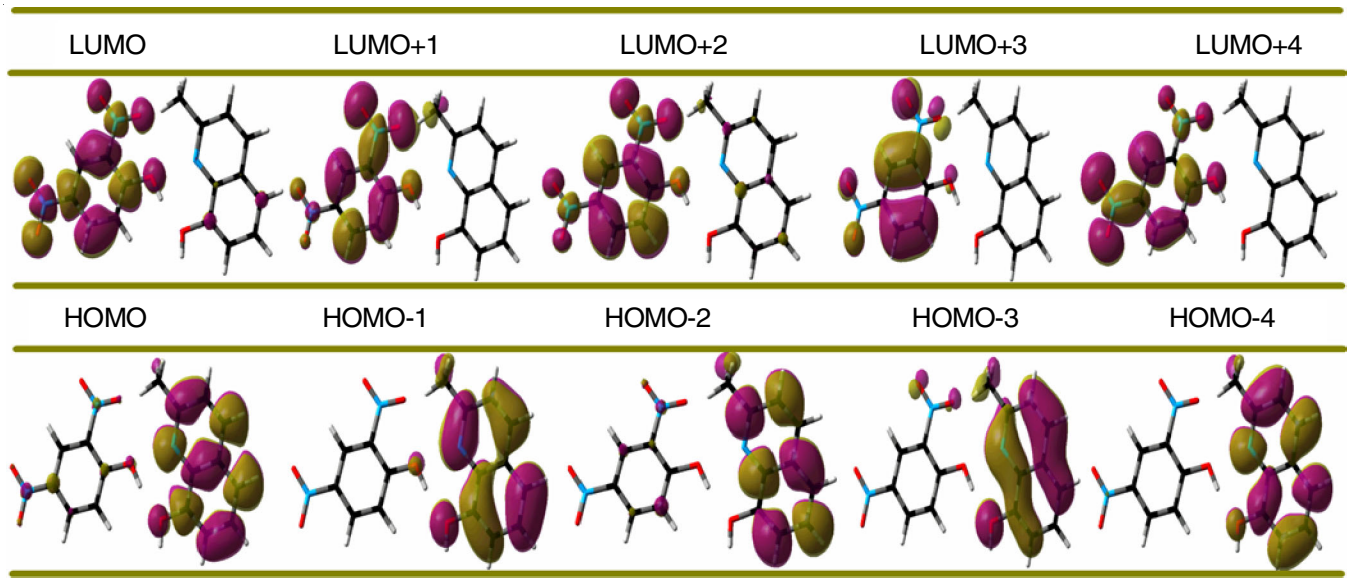

Fig. 10. FMO pictures of [(MHQ)(DNP)] complex calculated by DFT (CAM-B3LYP)

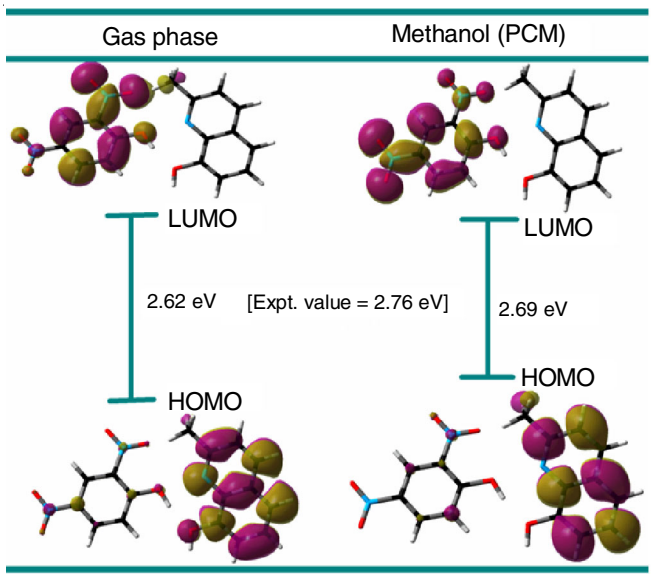

Fig. 11. HOMO-LUMO energy gaps of [(MHQ)(DNP)] complex in gas phase and PCM

HOMO and LUMO is illustrated. The LUMO is primarily concentrated on the DNP moiety, while the HOMO is exclusively found on the MHQ moiety. The complex MHQ region and N21 atomic orbital encompass the majority of the HOMO. Therefore, the n-electrons are confined to the HOMO molecular orbital. The LUMO represents a π* molecular orbital, whereas the other occupied molecular orbitals of the CT complex are found on the p-atomic orbitals of the quinoline moieties of MHQ and the experiments can be classified as n-π* and π-π* transitions.

Mulliken atomic charges: Fig. 12 present the Mulliken atomic charges of the donor, acceptor and [(MHQ):(DNP)] in both the gas and PCM. As a result of hydrogen bond growth, H-bond O16 expanded to -0.6227 a.u. in relation to the proton transfer from -0.5821 a.u. for free DNP. Conversely, for CT complex in gas phase, N21 increases to -0.64632 a.u. from -0.17831 a.u. (Table-7).

Reactivity parameters: The HOMO-LUMO surfaces can be used to calculate various reactivity descriptors that offer valuable insights into the reactivity of chemical reactions.

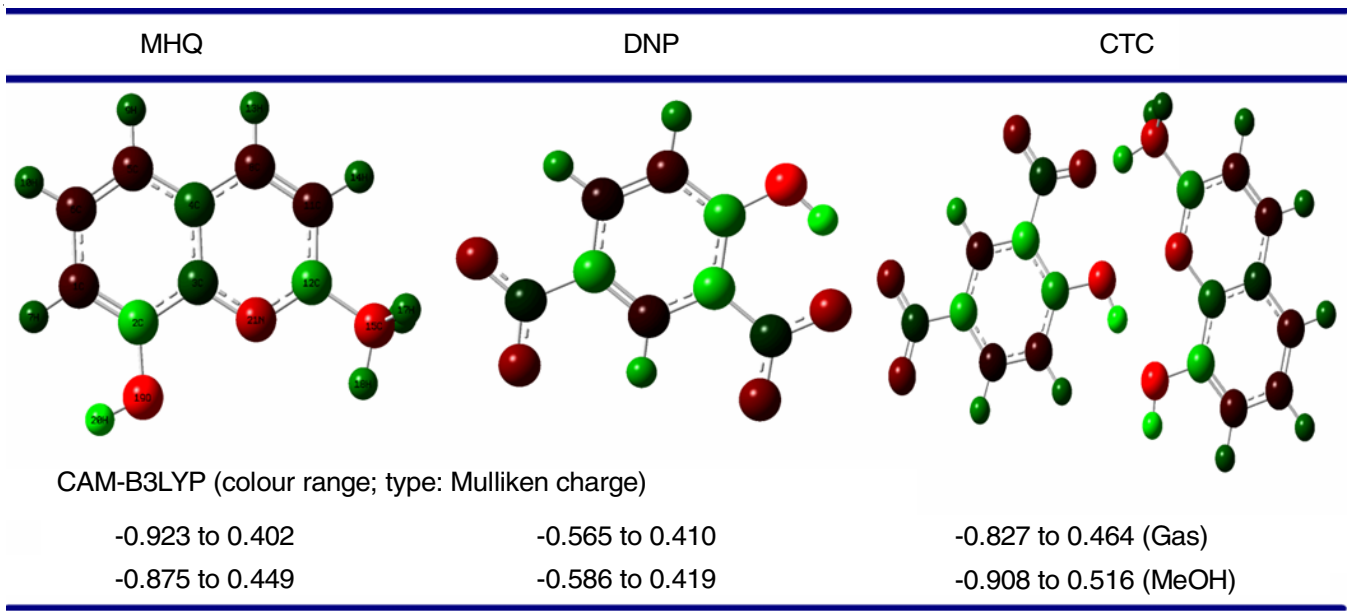

Fig. 12. Mulliken atomic charges of MHQ, DNP and CT complex in gas and PCM

TABLE-7
MULLIKEN ATOMIC CHARGE OF
MHQ, DNP AND [(MHQ)(DNP)] COMPLEX
CALCULATED USING THE CAM-B3LYP FUNCTION

Atom	MHQ	DNP	CTC	
			Gas	PCM
C1	0.03722	–	0.03746	0.042171
C2	-0.30248	–	-0.29985	-0.26785
C3	-0.09141	–	-0.09461	-0.07562
C4	0.31785	–	0.35806	0.39421
C5	0.33393	–	0.26909	0.21712
C6	-0.41502	–	-0.39057	-0.36125
C8	0.11206	–	0.14946	0.17546
O19	-0.80089	–	-0.82697	-0.87169
N13	-0.64632	–	-0.17831	-0.22436
C1	–	-0.07881	-0.08329	-0.11716
C2	–	0.27472	0.29708	-0.34568
C3	–	-0.09871	-0.10381	-0.17851
C4	–	0.30827	0.30221	0.31712
C5	–	0.27174	0.35141	0.37511
C6	–	-0.14121	-0.17116	-0.21577
N10	–	0.06584	0.04613	0.03711
O12	–	-0.25101	-0.29605	-0.31567
O14	–	-0.33506	-0.27903	-0.24562
N11	–	0.05679	0.04256	0.03756
O13	–	-0.30821	-0.28587	-0.26347
O15	–	-0.28264	-0.29369	-0.30648
H17	–	0.41841	0.46384	0.49517
O16	–	-0.58216	-0.66995	-0.70548

These descriptors include chemical potential (μ), ionization potential (IP), electron affinity (EA), hardness (η), softness (σ) and electrophilicity index (ω) [31]. The reactivity parameters' results showed that the molecule with the highest E_{HOMO} energy was the most effective electron-donor, whereas the molecule with the lowest E_{LUMO} energy was the best at accepting electrons (Table-8). In CT complex, MHQ served as an electronic donor and DNP as an electronic receiver. Using the chemical potential (μ) and electrophilicity index (ω) yielded the same results.

TABLE-8
REACTIVITY PARAMETERS OF MHQ
AND DNP GAS PHASE AND PCM

Parameter	Gas		PCM	
	MHQ	DNP	MHQ	DNP
E_{HOMO} (eV)	-6.86	-9.31	-5.19	-9.08
E_{LUMO} (eV)	-1.53	-4.26	-1.68	-2.46
I	6.86	9.31	5.19	9.08
A	1.53	4.26	1.68	2.46
η	2.66	2.57	1.75	3.31
μ	-4.19	-6.78	-3.43	-5.77
ω	3.16	9.11	3.36	5.02
σ	0.37	0.29	0.57	0.30

1 eV = 96.485 kJ mol^{-1}

Conclusion

A new hydrogen-bonded charge transfer (CT) complex obtained by combining electron-acceptor 2,4-dinitrophenol (DNP) with electron-donor 2-methyl-8-hydroxyquinoline (MHQ). The Job's and photometric methods clearly revealed that the physical composition had a 1:1 ratio. The presence of the H-bonded charge transfer (CT) complex was verified with ^{1}H NMR and FT-IR spectra, which were employed to characterize the synthesized solid complex. The SEM-EDX spectra have verified the surface morphology and elemental composition, indicating that the structure exhibits a sheet-like form. The DFT experiments further validated the presence of proton transfer prior to charge transfer, which explains the exceptional stability of the complex, and also supported the strong affinity in the CT complex. This evidence is derived from analyzing the geometrical parameters, Mullikan atomic charges, reactivity .

CONFLICT OF INTEREST

The authors declare that there is no conflict of interests regarding the publication of this article.

REFERENCES

1. R.S. Mulliken, *J. Am. Chem. Soc*., **74**, 811 (1952); https://doi.org/10.1021/ja01123a067
2. P.H. Emslie, R. Foster, I. Horman, J.W. Morris and D.R. Twiselton, *J. Chem. Soc. B*, 1161 (1969); https://doi.org/10.1039/j29690001161
3. K.M. Al-Ahmary, *Spectrochim. Acta A Mol. Biomol. Spectrosc.*, **117**, 635 (2014); https://doi.org/10.1016/j.saa.2013.09.008
4. V. Sundarpal, B.S. Kanth, N. Rajitha and B. Yadagiri, *Results Chem.*, **5**, 100694 (2023); https://doi.org/10.1016/j.rechem.2022.100694
5. A. Mostafa, G.B. Cieslinski and H.S. Bazzi, *J. Mol. Struct.*, **1081**, 136 (2015); https://doi.org/10.1016/j.molstruc.2014.09.074
6. H.S. Bazzi, A. Mostafa, S.Y. AlQaradawi and E.-M. Nour, *J. Mol. Struct.*, **842**, 1 (2007); https://doi.org/10.1016/j.molstruc.2006.12.005
7. G. Meesala, A.H. Syeda, M. Varukolu and P. Tigulla, *J. Indian Chem. Soc.*, **99**, 100799 (2022); https://doi.org/10.1016/j.jics.2022.100799
8. M. Sirajuddin, S. Ali and A. Badshah, *J. Photochem. Photobiol. B*, **124**, 1 (2013); https://doi.org/10.1016/j.jphotobiol.2013.03.013
9. G. Vadivelan, M. Saravanabhavan, V. Murugesan, G. Gohulvani, M. Sekar and B. Babu, *Mol. Cryst. Liq. Cryst.*, **652**, 242 (2017); https://doi.org/10.1080/15421406.2017.1378045
10. V. Mahipal, N. Venkatesh, B. Naveen, G. Suresh, V. Manaiah and T. Parthasarathy, *Chem. Data Coll.*, **28**, 100474 (2020); https://doi.org/10.1016/j.cdc.2020.100474
11. I.M. Khan, S. Shakya, M. Islam, S. Khan and H. Najnin, *Phys. Chem. Liq.*, **59**, 753 (2021); https://doi.org/10.1080/00319104.2020.1810250
12. K.M. Al-Ahmary, S.M. Soliman, M.M. Habeeb and A.H. Al-Obidan, *J. Mol. Struct.*, **1143**, 31 (2017); https://doi.org/10.1016/j.molstruc.2017.04.077
13. B. Mennucci, 2, 386 (2012); https://doi.org/10.1002/wcms.1086
14. R. Kobayashi and R.D. Amos, *Chem. Phys. Lett.*, **420**, 106 (2006); https://doi.org/10.1016/j.cplett.2005.12.040
15. Z.-L. Cai, M.J. Crossley, J.R. Reimers, R. Kobayashi and R.D. Amos, *J. Phys. Chem. B*, **110**, 15624 (2006); https://doi.org/10.1021/jp063376t
16. M. Varukolu, M. Kumar, P. Venkatesh, G. Manaiah, V. Parthasarathy, N. Suresh and P. Tigulla, *ACS Omega*, **7**, 810 (2022); https://doi.org/10.1021/acsomega.1c05464
17. A. Weyesa and E. Mulugeta, *RSC Adv.*, **10**, 20784 (2020); https://doi.org/10.1039/D0RA03763J
18. P. Manojkumar, Harilal, V. Mahipal, G. Suresh, N. Venkatesh, M. Ramesh and T. Parthasarathy, *RSC Adv.*, **11**, 39994 (2021); https://doi.org/10.1039/D1RA07658B
19. K.M. Al-Ahmary, M.M. Habeeb and E.A. Al-Solmy, *Phys. Chem. Liquids*, **51**, 131 (2013); https://doi.org/10.1080/00319104.2012.695072
20. M. Varukolu, M. Palnati, V. Nampally, S. Gangadhari, M. Vadluri and P. Tigulla, *ACS Omega*, **7**, 810 (2022); https://doi.org/10.1021/acsomega.1c05464
21. A. Tomberg, Gaussian 09W Tutorial, an Introduction to Computational Chemistry Using G09W and Avogadro Software, pp. 1-34 (2013).
22. M.J. Frisch, G.W. Trucks, H.B. Schlegel, G.E. Scuseria, M.A. Robb, J.R. Cheeseman, G. Scalmani, V. Barone, G.A. Petersson, H. Nakatsuji, X. Li, M. Caricato, A. Marenich, J. Bloino, B.G. Janesko, R. Gomperts, B. Mennucci, H.P. Hratchian, J.V. Ortiz, A.F. Izmaylov, J.L. Sonnenberg, D. Williams-Young, F. Ding, F. Lipparini, F. Egidi, J. Goings, B. Peng, A. Petrone, T. Henderson, D. Ranasinghe, V.G. Zakrzewski, J. Gao, N. Rega, G. Zheng, W. Liang, M. Hada, M. Ehara, K. Toyota, R. Fukuda, M. Ishida, J. Hasegawa, T. Nakajima, Y. Honda, O. Kitao, H. Nakai, T. Vreven, K. Throssell, J.A. Montgomery, Jr., J.E. Peralta, F. Ogliaro, M. Bearpark, J.J. Heyd, E. Brothers, K.N. Kudin, V.N. Staroverov, R. Kobayashi, T. Keith, J. Normand, K. Raghavachari, A. Rendell, J.C. Burant, J. Tomasi, S.S. Iyengar, M. Cossi, J.M. Millam, M. Klene, C. Adamo, R. Cammi, J.W. Ochterski, R.L. Martin, K. Morokuma, O. Farkas, J.B. Foresman, and D.J. Fox, Gaussian 09, Revision A.02, Gaussian, Inc., Wallingford CT (2016).
23. K.M. Al-Ahmary, M.M. Habeeb and A.H. Al-Obidan, *Spectrochim. Acta A Mol. Biomol. Spectrosc.*, **196**, 247 (2018); https://doi.org/10.1016/j.saa.2018.02.025
24. K.M. Al-Ahmary, M.M. Habeeb and E.A. Al-Solmy, *J. Mol. Liq.*, **162**, 129 (2011); https://doi.org/10.1016/j.molliq.2011.06.015
25. R.M. Alghanmi, S.M. Soliman, M.T. Basha and M.M. Habeeb, *J. Mol. Liq.*, **256**, 433 (2018); https://doi.org/10.1016/j.molliq.2018.02.056
26. H.A. Benesi and J. Hildebrand, *J. Am. Chem. Soc.*, **71**, 2703 (1949); https://doi.org/10.1021/ja01176a030
27. G. Briegleb, *Angew. Chem.*, **76**, 326 (1964); https://doi.org/10.1002/ange.19640760804
28. A.M.A. Adam, M. Salman, T. Sharshar and M.S. Refat, *Int. J. Electrochem. Sci.*, **8**, 1274 (2013); https://doi.org/10.1016/S1452-3981(23)14097-1
29. G. Briegleb, Elektronen Donator-Acceptor Komplexe, Springer-Verlag, Berlin (1961).
30. M. Gaber and S.S. Al-Shihry, *Spectrochim. Acta A Mol. Biomol. Spectrosc.*, **62**, 526 (2005); https://doi.org/10.1016/j.saa.2005.02.005
31. V. Nampally, M.K. Palnati, N. Baindla, M. Varukolu, S. Gangadhari and P. Tigulla, *ACS Omega*, **7**, 16689 (2022); https://doi.org/10.1021/acsomega.2c01177